International Journal of Nanomedicine

Dovepress

open access to scientific and medical research

Open Access Full Text Article

ORIGINAL RESEARCH

Glucose-Functionalized Silver Nanoparticles as a Potential New Therapy Agent Targeting Hormone-Resistant Prostate Cancer cells

Mariana Morais[1,2,*], Vera Machado[1,*], Francisca Dias[1], Patrícia Figueiredo[3], Carlos Palmeira[4–6], Gabriela Martins[4,5], Rui Fernandes[7,8], Ana Rita Malheiro[7,8], Kirsi S Mikkonen[3,9], Ana Luísa Teixeira[1,2], Rui Medeiros[1,2,6,10,11]

[1]Molecular Oncology and Viral Pathology Group, Research Center of IPO Porto (CI-IPOP)/RISE@CI-IPOP (Health Research Network), Portuguese Oncology Institute of Porto (IPO Porto)/Porto Comprehensive Cancer Center (Porto.CCC), Research Center-LAB2, Porto, 4200-072, Portugal; [2]ICBAS, Abel Salazar Institute for the Biomedical Sciences, University of Porto, Porto, 4050-513, Portugal; [3]Department of Food and Nutrition, Faculty of Agriculture and Forestry, University of Helsinki, Helsinki, FI-00014, Finland; [4]Department of Immunology, Portuguese Oncology Institute of Porto (IPO-Porto), Porto, 4200-072, Portugal; [5]Experimental Pathology and Therapeutics Group, Research Center of IPO Porto (CI-IPOP)/RISE@CI-IPOP (Health Research Network), Portuguese Oncology Institute of Porto (IPO Porto)/Porto Comprehensive Cancer Center (Porto.CCC), Research Center-LAB2, Porto, 4200-072, Portugal; [6]Biomedical Research Center (CEBIMED, Faculty of Health Sciences, Fernando Pessoa University (UFP), Porto, 4249-004, Portugal; [7]HEMS-Histology and Electron Microscopy, i3S-Instituto de Investigação e Inovação em Saúde, University of Porto, Porto, 4200-135, Portugal; [8]IBMC, Instituto de Biologia Molecular e Celular da Universidade do Porto, Porto, Portugal; [9]Helsinki Institute of Sustainability Science (HELSUS), University of Helsinki, Helsinki, FI-00014, Finland; [10]Research Department, LPCC- Portuguese League Against Cancer (NRNorte), Porto, Portugal; [11]Faculty of Medicine, University of Porto (FMUP), Alameda Prof. Hernâni Monteiro, University of Porto, Porto, 4200-319, Portugal

*These authors contributed equally to this work

Correspondence: Rui Medeiros; Ana Luísa Teixeira, Molecular Oncology and Viral Pathology Group, Research Center of IPO Porto (CI-IPOP) /RISE@CI-IPOP (Health Research Network), Portuguese Oncology Institute of Porto (IPO Porto)/Porto Comprehensive Cancer Center (Porto. CCC), Research Center-LAB2, E Bdg 1st floor, Rua Dr António Bernardino de Almeida, Porto, 4200-072, Portugal, Tel +351 225 084 000 Ext:5115, Fax +351 225 084 001, Email ruimedei@ipoporto.min-saude.pt; ana.luisa.teixeira@ipoporto.min-saude.pt

Purpose: Silver nanoparticles (AgNPs) have shown great potential as anticancer agents, namely in therapies' resistant forms of cancer. The progression of prostate cancer (PCa) to resistant forms of the disease (castration-resistant PCa, CRPC) is associated with poor prognosis and life quality, with current limited therapeutic options. CRPC is characterized by a high glucose consumption, which poses as an opportunity to direct AgNPs to these cancer cells. Thus, this study explores the effect of glucose functionalization of AgNPs in PCa and CRPC cell lines (LNCaP, Du-145 and PC-3).

Methods: AgNPs were synthesized, further functionalized, and their physical and chemical composition was characterized both in water and in culture medium, through UV-visible spectrum, dynamic light scattering (DLS), transmission electron microscopy (TEM) and Fourier-transform infrared spectroscopy (FTIR). Their effect was assessed in the cell lines regarding AgNPs' entering pathway, cellular proliferation capacity, ROS production, mitochondrial membrane depolarization, cell cycle analysis and apoptosis evaluation.

Results: AgNPs displayed an average size of 61nm and moderate monodispersity with a slight increase after functionalization, and a round shape. These characteristics remained stable when redispersed in culture medium. Both AgNPs and G-AgNPs were cytotoxic only to CRPC cells and not to hormone-sensitive ones and their effect was higher after functionalization showing the potential of glucose to favor AgNPs' uptake by cancer cells. Entering through endocytosis and being encapsulated in lysosomes, the NPs increased the ROS, inducing mitochondrial damage, and arresting cell cycle in S Phase, therefore blocking proliferation, and inducing apoptosis.

Conclusion: The nanoparticles synthesized in the present study revealed good characteristics and stability for administration to cancer cells. Their uptake through endocytosis leads to promising cytotoxic effects towards CRPC cells, revealing the potential of G-AgNPs as a future therapeutic approach to improve the management of patients with PCa resistant to hormone therapy or metastatic disease.

Keywords: castration-resistant prostate cancer, hormonal therapy, therapy resistance, Warburg Effect

Received: 8 March 2022
Accepted: 17 May 2022
Published: 16 September 2022

Plain Language Summary

Prostate cancer (PCa) is the second most frequent and the fifth cause of cancer-related death in men worldwide. When patients stop responding to androgen deprivation therapy, they progress to castration-resistant prostate cancer (CRPC), which is associated with poor prognosis and limited therapeutic options. Thus, the present study evaluated the cytotoxic potential of silver nanoparticles (AgNPs) functionalized with glucosamine in PCa cell lines, since in the last years, several researchers have shown that AgNPs can be useful as anticancer drugs. In our study, we successfully synthesized and functionalized AgNPs and we proved them to be stable in cell culture medium, which is important because they can remain in circulation intact until they get to tumor location. We observed that AgNPs were cytotoxic to CRPC cell lines and not to the sensitive ones and that glucosamine functionalization increased their cytotoxic capacity. With this study, we showed that the nanoparticles enter the cells through endocytosis and increase the production of reactive oxygen species, inducing damage in mitochondria. The damage induced by the nanoparticles lead to a blockage of cell cycle and, consequently, of cell proliferation inducing apoptosis. These results reveal the potential of glucosamine functionalized AgNPs as a future therapeutic approach to improve the management of patients with CRPC or metastatic disease.

Introduction

Prostate cancer (PCa) is the second most frequent and the fifth cause of cancer-related death in men worldwide.[1,2] Nearly 79% of the patients are diagnosed at an early and localized stage but, 35–60% of these patients experience disease recurrence.[3] In cases of advanced disease, androgen deprivation therapy (ADT) is the first-line treatment, suppressing AR signalling and inhibiting PCa cells' proliferation.[4] Despite the high early response rates, the heterogeneity of PCa cells ultimately leads to their adaptation to androgen deprivation and reactivation of AR signalling even under a low level of serum androgen with patients progressing to castration-resistant prostate cancer (CRPC) within 2 to 3 years.[5] Progression to CRPC is burdened with poor prognosis and impaired quality of life, being the estimated mean survival of these patients 15–36 months.[6,7] In the last years, the upcoming of second-generation antiandrogens (such as enzalutamide and abiraterone), chemotherapy (such as docetaxel and cabazitaxel) and radionuclide therapy (radium-223) have improved overall survival (OS).[8] Nevertheless, the increase in the median PCa-specific survival in mCRPC with the introduction of the novel therapies only increases 2.8–4.8 months, making overcoming resistance one of the major challenges in these patients' management.[9–11]

There are different molecular mechanisms behind the acquisition of resistance to ADT.[6] Among them is the disruption of glucose metabolism, since AR regulates genes related to glucose consumption and increases the activity of several glycolytic enzymes. One example of such is GLUT1′s expression, which is associated with poor prognosis and whose gene promotor directly binds to AR.[12–15] Prostate cells show, indeed, a distinctive metabolism, with unique alterations during tumor development and progression.[16] Due to the prostate epithelial cells' function of producing and secreting citrate that will be part of the seminal fluid, in normal conditions, Krebs cycle is interrupted and cells produce energy mostly through a glycolytic pathway.[17] During tumor development, Krebs cycle is reactivated in consequence of the cancer cells higher energetic demands.[18] In the most advanced stages of the disease, there is a preference for cancer cells to metabolize glucose through glycolysis and lactate fermentation instead of Krebs cycle and oxidative phosphorylation, also called the Warburg Effect.[19] This is a faster method to obtain energy and acidifies the microenvironment of the tumor; however, it is energetically inefficient. Therefore, it is normally followed by an increase in glucose consumption by cancer cells.[20] This increased glucose uptake poses as an opportunity of targeting CRPC cells in the development of new therapy approaches.

The steady development of nanotechnology and nanoscience in the last years has brought up a particular interest in the development of metallic nanoparticles directed to biotechnology and biomedicine in different medical fields, including oncology, with various nanoparticles (NPs) having been approved for clinical use, either by the Food and Drug Administration in the United States or the European Medicines Agency (EMA) in the European Union.[21–23] Due to their nanoscale size, high surface-to-volume ratio, different chemical composition and the ability to attach different targeting ligands to their surfaces, silver nanoparticles (AgNPs), which are small, organized structures ranging from 1 to 100 nm in size with about 20–15,000 atoms, have been emerging as a potential strategy to improve treatment in different tumor models, including the overcome of therapy-resistant cancer phenotypes.[24,25] In fact, AgNPs nanoscale size allows them to cross tissue barriers since the tissue junction between capillaries ranges from 150 to 200 μM. Moreover, while

larger particles (>200 nm) accumulate in the liver and spleen, being quickly removed from the bloodstream by macrophages of the reticuloendothelial system, smaller AgNPs are limited to tissue extravasation and renal clearance.[23] When inside the tumor cells, they trigger different processes that result in the activation of signaling pathways that lead to apoptosis.[25,26] These characteristics show AgNPs' potential as anticancer agents, for example, in therapies' resistant forms of cancer. Their long-term toxicity is yet not fully understood, with contradictory data having been presented throughout the years. Nevertheless, in a recent review, Ivlieva and collaborators concluded that the toxicity is mostly due to the liberation of Ag^+ and not from the nanoparticle itself, showing the importance of a good stability of the AgNPs for its safety.[27] Additionally, Maziero and her team have shown that AgNPs stabilized with Gum Arabic Protein revealed adverse effects in zebrafish species but not in Sprague Dawley rats for 28 days in doses up to 10.0 mg/kg which shows the potential of their usage and the importance of their study.[28] Thus, the purpose of this study was to synthesize and characterize AgNPs functionalized with glucose (G-AgNPs) and further study their cytotoxic and cellular effect in PCa cells resistant to ADT.

Materials and Methods

Materials

Silver nitrate ≥99% ($AgNO_3$), sodium citrate dihydrate, tannic acid, and D-(+)-glucosamine hydrochloride were purchased in Sigma-Aldrich. Roswell Park Memorial Institute-1640 medium (RPMI-1640), fetal bovine serum (FBS), penicillin–streptomycin and trypsin-EDTA were purchased from Gibco®. Trypan Blue, which allows for the evaluation of cytoplasmic membrane damage, was purchased from VWRTM. Resazurin, which allows for the evaluation of cell viability and IC_{50} determination was purchased from ACROS Organic™ – Fisher Scientific®. Bromodeoxyuridine (BrdU), which allows for the evaluation of cell proliferation capacity, was purchased from ROCHE®. Propidium iodide (PI), which allows for the evaluation of cell cycle, was purchased from Sigma-Aldrich®. Tetramethylrhodamine (TMRE) kit, which allows for the evaluation of mitochondrial membrane potential, was purchased from Abcam®. The 2',7'-dichlorodihydrofluorescein diacetate (H_2DCFDA), which allows to quantitatively assess reactive oxygen species, was purchased from Millipore®.

Synthesis of AgNPs

An aqueous solution containing 5 mM sodium citrate and 5 mM tannic acid at final volume of 100 mL was mixed and heated at 100 °C, for 15 min under vigorous stirring, as described by Bastus et al.[29] After starting to boil, 1 mL of 25 mM $AgNO_3$ was added into this solution. The resulting AgNPs were purified by centrifugation at 20,000 g for 15 min and further redispersed in MilliQ (MQ) water.

Functionalization of AgNPs with Glucosamine

After synthesis, the functionalization of AgNPs with glucosamine was done by ligand exchange.[29] For that, 1 mg of AgNPs was redispersed with 2 mL of 2 mM sodium citrate containing 5 mM glucosamine hydrochloride, and the solution was stirred for 24 h at room temperature. Finally, the resulting G-AgNPs were washed, redispersed in MQ-water, and stored at 4 °C.

Characterization of AgNPs

The average hydrodynamic diameter, polydispersity index, and ζ-potential of the AgNPs were measured by dynamic light scattering (DLS), using a Malvern Zetasizer Nano ZS instrument (Malvern Instruments Ltd, UK). For this, the samples were diluted in MilliQ-water at concentration of 100 µg/mL. The morphology of AgNPs was confirmed by transmission electron microscopy (TEM, Jeol JEM-1400, Jeol Ltd., Tokyo, Japan), using an acceleration voltage of 80 kV. For the sample preparation, a droplet of AgNPs' suspension was placed on a carbon-coated copper grid, blotted using a filter paper, and then air-dried before analysis. To acquire the UV–visible spectra, AgNP dispersions at concentration of 15 µg/mL were placed in a cell, and the analysis was performed in the 300–700 nm range at room temperature, using an UV-visible spectrophotometer (UV-1800 Shimadzu) with the UV probe 2.70 software. Additionally, the AgNPs were characterized using a Fourier transform infrared spectroscopy (FTIR) instrument (SpectrumOne, PerkinElmer, Turku, Finland), equipped with a universal attenuated total reflectance (ATR) accessory. The ATR-FTIR spectra were recorded at

room temperature between 4000 and 600 cm^{-1} with a resolution of 4 cm^{-1} and number of 64 scans, and the baseline was corrected using the built-in software. The stability of AgNPs was evaluated after incubation of 500 μg/mL of AgNPs with RPMI supplemented with 10% fetal bovine serum (FBS), at 37 °C for 2 h. For this, 200 μL were withdrawn at 5, 15, 30, 60, 90 and 120 min, and diluted in water to evaluate changes on the size, PDI and ζ-potential of AgNPs over time. All the experiments were performed in triplicates.

Cell Culture and Treatments Conditions

PC-3 and LNCaP cells (ATCC® CRL-1435™ RRID:CVCL 0035 and ATCC® CRL-1740™ RRID:CVCL_1379, respectively) were obtained from ATCC and Du-145 cells (ATCC® HTB-81: RRID:CVCL_0105) were kindly granted by Professor Cármen Jerónimo from IPO-Porto Research Center (Portugal). Cells were cultured in RPMI-1640 medium supplemented with 10% fetal bovine serum (FBS) and 1% penicillin-streptomycin and were maintained in a humidified incubator at 37°C, 5% CO_2 and 95% humidity. Cells were routinely grown in tissue culture flasks and harvested with a solution of trypsin-EDTA 0.05% (Gibco®, Gaithersburg, MD, USA), while in a logarithmic growth phase. When cells had reached 80–90% confluence, cells were trypsinized with trypsin-EDTA 0.05% (Gibco®, Gaithersburg, MD, USA). The cell pellets were resuspended in growth media, and cells were counted using trypan blue solution (VWR™) and an automatic cell counter (EVE™ – NanoEntek). All cell lines were routinely tested, each 2 weeks, for mycoplasma presence and were found to be free from contamination.

AgNPs and G-AgNPs IC_{25} and IC_{50} Determination by Resazurin Assay

Cells were cultured in 96-multi-well plates at a density of 2×10^5 cells per mL and treated with increasing concentrations of AgNPs and G-AgNPs, ranging from 600 to 3000μg/mL for 24h. Then, cells' viability was determined by a cell viability assay using Resazurin sodium salt (ACROS Organic™ – Fisher Scientific®, MA, USA). Two biological replicates were made for all the conditions, with seven technical replicates each. The IC_{50} of both AgNPs and G-AgNPs was determined using The Quest Graph™ IC_{50} Calculator, with a four-parameter logistic regression model, using the seven replicates and the average of the IC_{50} was calculated. The same was done for the IC_{25} determination, using the following equation: $IC25 = \left(\frac{25}{100-25}\right)^{\frac{1}{\text{Hill Slope}}} \times IC50$. The following assays were made using the IC_{25} and IC_{50} values determined for each cell line.

Determination of Cellular Localization of AgNPs and G-AgNPs by Transmission Electron Microscopy (TEM)

Cells were cultured in 6-multi-well plates at a density of 2×10^5 cells per mL and treated with the determined IC_{25} for 24 hours. Then, cells were harvested with a solution of trypsin-EDTA and fixated. Cells were then further processed, and TEM images were collected by the Histology and Electron Microscopy platform from I3S Porto using a Jeol JEM 1400 Transmission Electron Microscope.

Cell Proliferation Assay – BrdU

BrdU assay was performed to evaluate cell proliferation. During the assay, BrdU, which is an analog of the nucleoside thymidine, is incorporated into replicating DNA, thus being an indicator of cellular proliferation. BrdU assay was performed using the Cell Proliferation ELISA, BrdU kit, according to the manufacturer instructions (Roche Diagnostics®, Germany). Briefly, cells were grown overnight in 96-well microplates and incubated with either AgNPs or G-AgNPs and 5'-bromodeoxyuridine (BrdU) solution at a final concentration of 0.01 mM for 24 h. The optical density of proliferating cells (positive for BrdU) after ELISA assay using anti-BrdU-specific antibodies was evaluated at the microplate reader (FLUOstar Omega, BMG Labtech, Ortenberg Germany). Results were expressed as percentage of control (100%). Two biological replicates and five technical replicates were performed for each condition.

Cell Cycle Analysis

Cell cycle analysis was performed by measuring the DNA content of the treated and untreated cells using Propidium Iodide (PI) by flow cytometry. Briefly, cells were grown in 6-well plates (2 wells per condition) and incubated with AgNPs and G-AgNPs for 24 hours. Then, culture medium was collected, and the cells detached with trypsin/EDTA and centrifuged at 160 g for 3 minutes. The pellet was washed with PBS 1× (Gibco®, Gaithersburg, MD, USA) and fixed by slowly adding 3 mL of cold 70% (v/v) ethanol for 15 minutes at 4°C. Fixed cells were centrifuged and the pellet obtained was washed with cold PBS. Subsequently, the cells were stained with a solution containing Triton X-100 (1.1%, v/v), PI and RNase A (50 and 100 µg/mL, respectively) in PBS. The cell cycle analysis was made using the Cytomics FC500 flow cytometer (Beckman Coulter) and the CXP software. The percentage of cells in the sub-G1 phase of the cell cycle was calculated from the total 10,000 cells (100%) in the assay, and the percentage of cells in G0/G1, S and G2/M phases was calculated from the total cells excluding the sub-G1 cells. Three technical replicates were performed for each condition.

Cell Apoptosis Assay – FITC Annexin V and PI

Apoptosis was evaluated through the Annexin V-FITC Apoptosis Detection kit (Abcam) according to manufacturer's protocol. Briefly, cells were grown in 6-well plates (2 wells per condition) and incubated with AgNPs and G-AgNPs for 24 hours. Then, cells were detached using Accutase enzyme cell detachment medium (Thermo Fisher Scientific) and stained with both recombinant annexin V conjugated to fluorescein (FITC annexin V) and red-fluorescent propidium iodide (PI) nucleic acid binding dye. Data analysis was performed through CXP Software in a FC500 Beckman Coulter flow cytometer.

Detection of Intracellular Reactive Oxygen Species – $DCFH_2$-DA Assay

Intracellular ROS formation was assessed by measuring the fluorescence of DCF, the oxidation product of the non-fluorescent probe 2',7'-dichlorodihydrofluorescein diacetate ($DCFH_2$-DA). Briefly, cells were grown in 96-well plates at a density of 2.0×10^5 cells per mL were treated with the IC_{25} and IC_{50} of AgNPs and G-AgNPs for 24h. Three hours prior to completion of treatment, 150 µM *tert*-butyl hydrogen peroxide (Sigma-Aldrich®, USA) was used as positive control. Then, cells were incubated with 10 µM DCFH2-DA (Merck Millipore®, USA) for 30 minutes at 37 °C, in the dark. Live cells were then imaged with filter set appropriate for fluorescein (FITC) using a fluorescence microscope OLYMPUS IX51 (Tokyo, Japan). The oxidation of $DCFH_2$-DA was detected by the increase in fluorescence which is proportional to the amount of intracellular ROS generated. The intracellular mean fluorescence intensity was quantified using the ImageJ software (National Institutes of Health, USA).

Mitochondrial Membrane Potential Assay (TMRE)

To assess the alterations on mitochondrial membrane potential, an important parameter of mitochondrial function used as an indicator of cell death, active mitochondria were labeled with tetramethylrhodamine, ethyl ester (TMRE) (Abcam, Cambridge, UK) according to the manufacturer's instructions. Cells were plated in 96-well plates with clear flat bottom and black sides at a density of 2.0×10^5 cells per mL and treated with the IC_{25} and IC_{50} of AgNPs and G-AgNPs for 24h. A positive control, carbonyl cyanide-p-trifluoromethoxyphenylhydrazone (FCCP), an uncoupler of mitochondrial oxidative phosphorylation, was used at the concentration of 100 µM for 10 minutes. After that, the cells were incubated with 500 nM of TMRE for 20 minutes at 37 °C, 5% CO_2, followed by one washing step with 100 µL of PBS containing 0.2% bovine serum albumin (BSA). A volume of 100 µL of PBS/0.2% BSA was added to each well, and the fluorescence was measured in a microplate fluorescence reader (Flx 800, Biotek) with excitation/emission: 549/575 nm. After background subtraction, the results were expressed as percentage of control (100%). Additionally, live cells were imaged with filter set appropriate for tetramethylrhodamine (TRITC) using a fluorescence microscope OLYMPUS IX51 (Tokyo, Japan). Two biological replicates and five technical replicates were performed for each condition.

Statistical Analysis

Using the sample *t*-test, the Mann–Whitney and the Kruskal–Wallis tests (depending on whether the results followed or not a normal distribution), the results were analyzed using SPSS26 software (release 26, SPSS Inc., Chicago, IL/USA) and their graphical representation was constructed using GraphPad Prism 6 software. p-values <0.05 were considered statistically significant.

Results

Synthesis and Characterization of AgNPs

To synthesize the AgNPs, sodium citrate and tannic acid were used as reducing agents, as previously done by Bastús et al.[29] After adding the aqueous solution of silver nitrate ($AgNO_3$) into the previous mixture, the solution changed its color from light yellow to dark brown within minutes, indicating the presence of AgNPs. The AgNPs were centrifuged and washed with MQ water before redispersing them with MilliQ (MQ) water. The ligand exchange of the resulting AgNPs with the amino-terminated glucose molecule (glucosamine) was performed in order to functionalize the AgNPs with glucose (G-AgNPs).[29] For that, the as-prepared AgNPs were mixed with glucosamine in a sodium citrate solution under vigorous stirring, and further centrifuged and washed to remove the excess of glucosamine. This ligand exchange is a spontaneous reaction that occurs due to the strong bonds formed between the amino groups on the glucosamine and the COOH/OH groups in the citrate/tannic molecules on the AgNP surface.[29] In addition, the plain AgNPs were also incubated in sodium citrate as control. The resulting AgNPs were further characterized by dynamic light scattering (DLS), transmission electron microscopy (TEM), UV–Vis spectroscopy, and Fourier transform infrared spectroscopy (FTIR) (Figure 1).

The molar ratio of tannic acid and sodium citrate (1:1) used in the AgNP synthesis was chosen to obtain AgNPs with an average size of 61 ± 10 nm and moderate monodispersity (Figure 1A), given by their PDI values lower than 0.25. The surface charge of plain AgNPs was highly negative (–59 ± 6 mV), mainly due to the free COOH/OH groups of tannic acid and sodium citrate on the AgNP surface (Figure 1B). After functionalization with glucosamine, the size of G-AgNPs (64 ± 11 nm) and PDI did not change significantly. However, the ζ-potential of G-AgNPs slightly increased (–50 ± 4 mV), which indicates some replacement of sodium citrate/tannic acid by glucosamine. The optical characterization of the AgNPs (Figure 1C) showed a maximum UV-Vis absorption at around 412 nm due to the surface plasmon resonance.[30] Moreover, the G-AgNPs presented a red-shift in surface plasmon resonance band at 563 nm, suggesting a small increase in the size and polydispersity of the functionalized AgNPs.[29,30] Besides the effect on reducing the polydispersity of AgNPs, the addition of high molar amount of tannic acid also influences the morphology of the resulting AgNPs. The TEM images showed that AgNPs presented roughly round shape (Figure 1D), because of the high amount of tannic acid added to the reaction mixture for the AgNP synthesis.[29] The FTIR analysis was also conducted in order to determine the functional groups present on the surface of the AgNPs and evaluate the differences between the plain AgNPs and the glucosamine-functionalized AgNPs (Figure 1E). The G-AgNPs spectrum showed stretching vibrations of C–H bonds from CH_2 groups at 2980 and 2900 cm^{-1}, C–N stretch on aromatic amines at 1390 cm^{-1}, stretching of the glycosidic linkage (C–O–C) and C–OH in the sugar ring at 1245 cm^{-1}, and deformation vibrations of C–O bonds in secondary alcohols at 1065 cm^{-1}.[31,32] Therefore, these results suggested that the functionalization of AgNPs with glucosamine was successful.

Evaluation of the AgNP Stability

The synthesized NPs are known to remain stable dispersed in water for over a month. However, the magnitude and specificity of protein adsorption onto the surface of NPs in physiological environment can be influenced by the composition, size, shape and surface charge of the particles, which will ultimately affect their cellular uptake and biodistribution.[33,34] Therefore, it is important to study its stability in these conditions. Since adsorption of proteins of nanoparticles usually happens in the first minutes of incubation, we performed a stability test of AgNPs and G-AgNPs for up to 2 hours. In this way, the stability of the AgNPs was evaluated in relevant biological media by measuring the changes on the size, PDI and ζ-potential of the NPs. For that, the AgNPs were incubated in RPMI, supplemented with

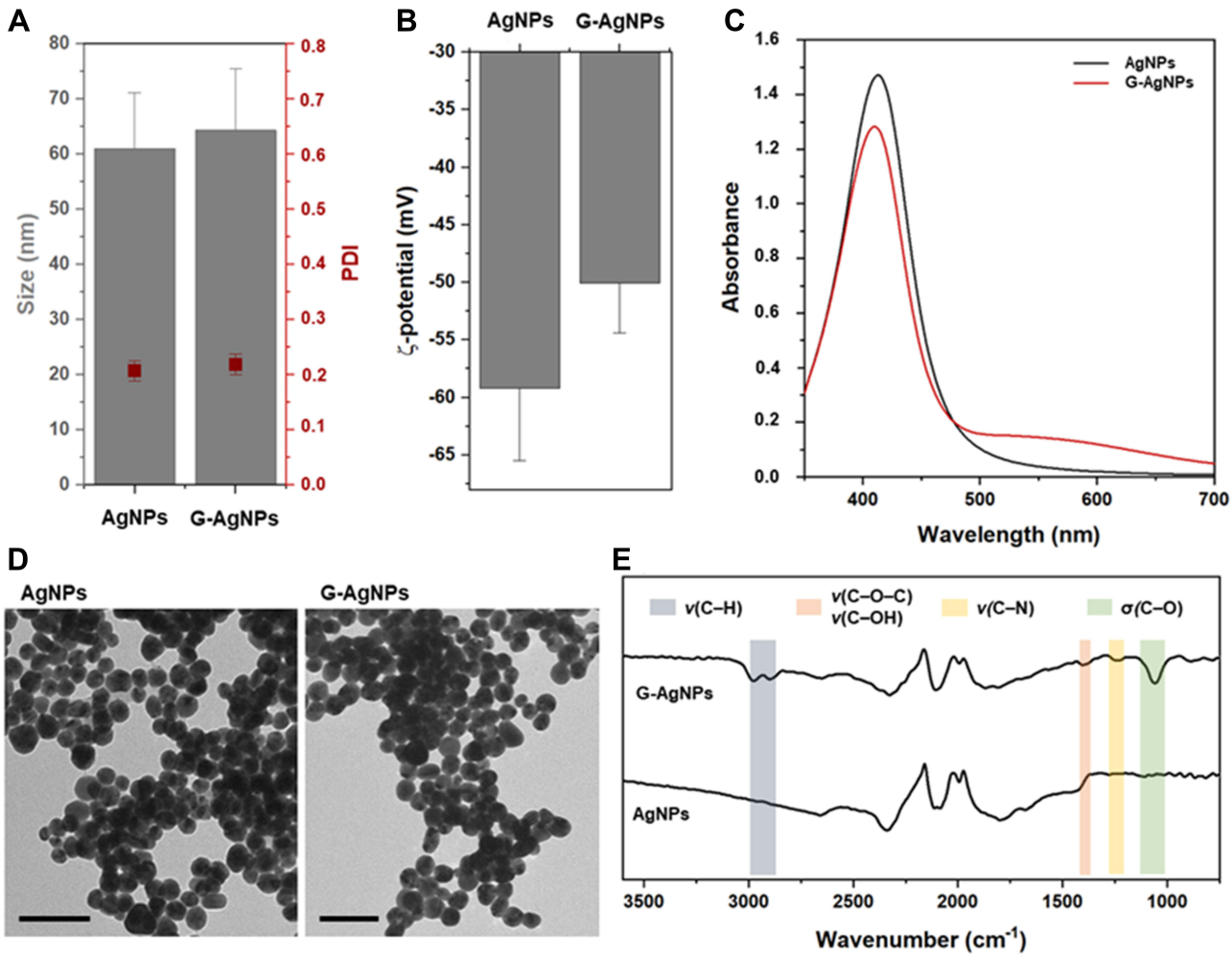

Figure 1 Characterization of AgNPs and G-AgNPs by means of (**A**) Size and PDI; (**B**) ζ-potential, and (**C**) UV-Vis spectra. (**D**) TEM images of AgNPs and G-AgNPs (Scale bars = 100 nm). (**E**) ATR-FTIR spectra of AgNPs and G-AgNPs. Error bars represent mean ± SD (n ≥ 3).

10% of FBS at 37 °C, for 2 h (Figure 2). In the first 30 min of incubation, a slight increase in the NP size from ca. 60 nm to 110 and 100 nm for AgNPs and G-AgNPs, respectively, indicating some protein adsorption onto the NPs' surface due to the FBS proteins (Figure 2A). Furthermore, the size of the AgNPs kept constant over time, along with steady PDI values (Figure 2B), suggesting that the AgNPs remained monodispersed after incubation with the FBS containing cell culture medium. In addition, the surface charge of the NPs shifted to about –17 mV after the first 5 min of incubation, due to the protein adsorption on their surface. Overall, the stability of AgNPs can be ascribed to the presence of FBS in cell culture medium that can improve the colloidal stability of NPs.[34,35]

IC_{25} and IC_{50} Determination

To perform the in vitro study, three cell lines were used: one hormone-sensitive cell line, LNCaP and two AR- and hormone-resistant cell lines Du-145 and PC-3. The cytotoxic effect of both AgNPs and G-AgNPs in the three cell lines used in the study was determined using the resazurin assay, and IC_{25} and IC_{50} were calculated. Regarding the LNCaP cell line, it was not possible to determine the IC_{25} and IC_{50} since there was no consistent effect of both AgNPs and G-AgNPs in these cells (Figure 3A). Regarding Du-145 and PC-3 cell lines, one can see that the viability of both cell lines decreases with the increase in both AgNPs' and G-AgNPs' concentration (Figure 3B and C), thus allowing the determination of the IC_{25} and IC_{50} (Table 1).

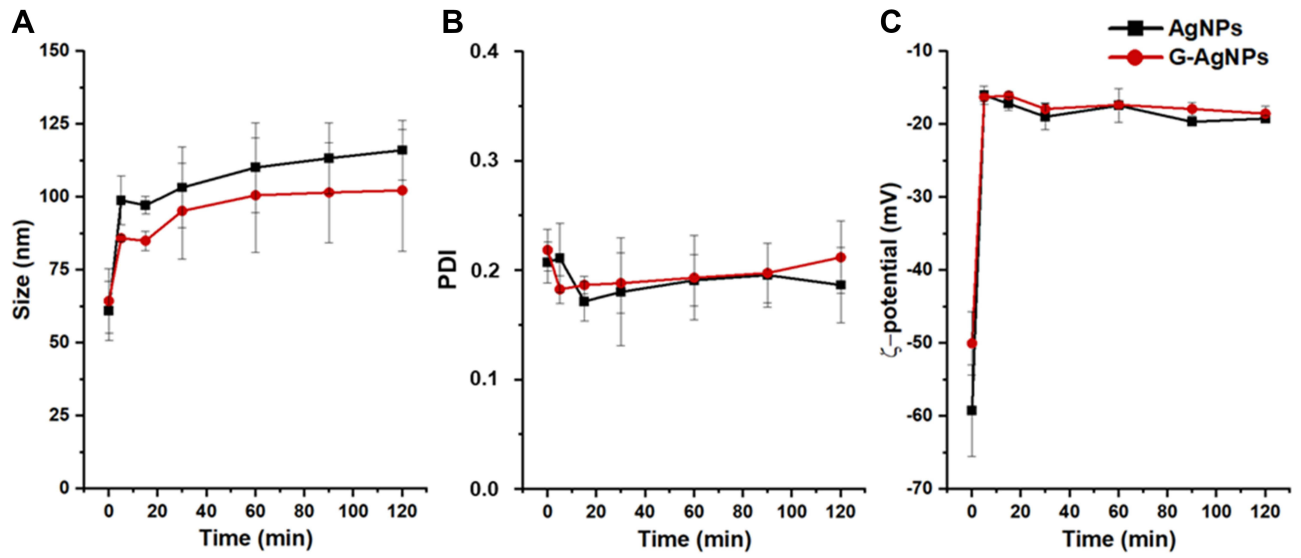

Figure 2 Stability of AgNPs in RPMI supplemented with 10% of FBS after 2 h incubation, at 37 °C: effect on the size (**A**), PDI (**B**) and ζ-potential (**C**) of AgNPs. Errors bars represent mean ± SD (n = 3).

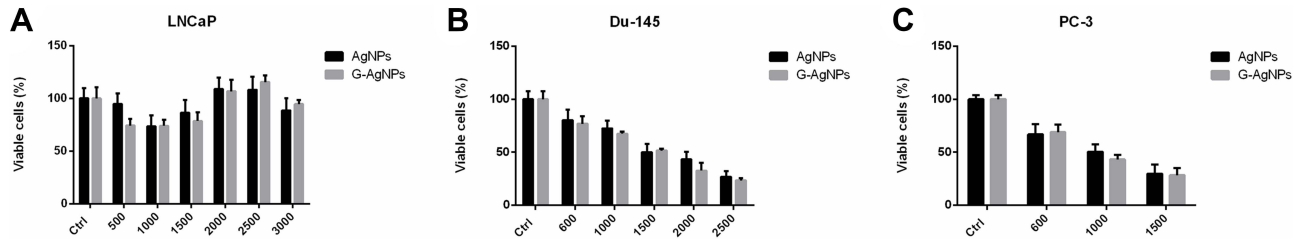

Figure 3 Evaluation of cell viability, by Resazurin Assay, upon treatment with AgNPs and G-AgNPs for 24 hours in LNCaP cell line (**A**) Du-145 cell line (**B**) and PC-3 cell line (**C**). Results are expressed as percentage of control (untreated cells), as mean ± SEM.

It is important to note that for both cell lines, the IC_{25} and IC_{50} are lower for G-AgNPs than AgNPs, suggesting an increased cytotoxic effect of the AgNPs after functionalization (Table 1). Moreover, both IC_{25} and IC_{50} in AgNPs and G-AgNPs are lower in PC-3 cell line when compared to Du-145. The determined values of IC_{25} and IC_{50} were then used in the following phenotypic assays.

AgNPs and G-AgNPs Intracellular Localization

To further confirm AgNPs and G-AgNPs internalization by both Du-145 and PC-3 cells, we performed a TEM analysis after administration of AgNPs (Figure 4A–C and H–J) and G-AgNPs (Figure 4D–G and K–M) at IC_{25}, to Du-145 and PC-3, respectively (Figure 4). One can observe that nanoparticles enter the cells through endocytosis (Figure 4J-1) and are trapped in lysosomes (Figure 4J-2). Inside the cell, they seem to be dispersed, since they can be observed in the

Table 1 IC_{25} and IC_{50} of AgNPs and G-AgNPs in Du-145 and PC-3 Cell Lines

Cell Line	Silver Nanoparticles	IC_{25} (μg/mL)	IC_{50} (μg/mL)
Du-145	AgNPs	919	1579
	G-AgNPs	753	1528
PC-3	AgNPs	511	911
	G-AGNPs	499	860

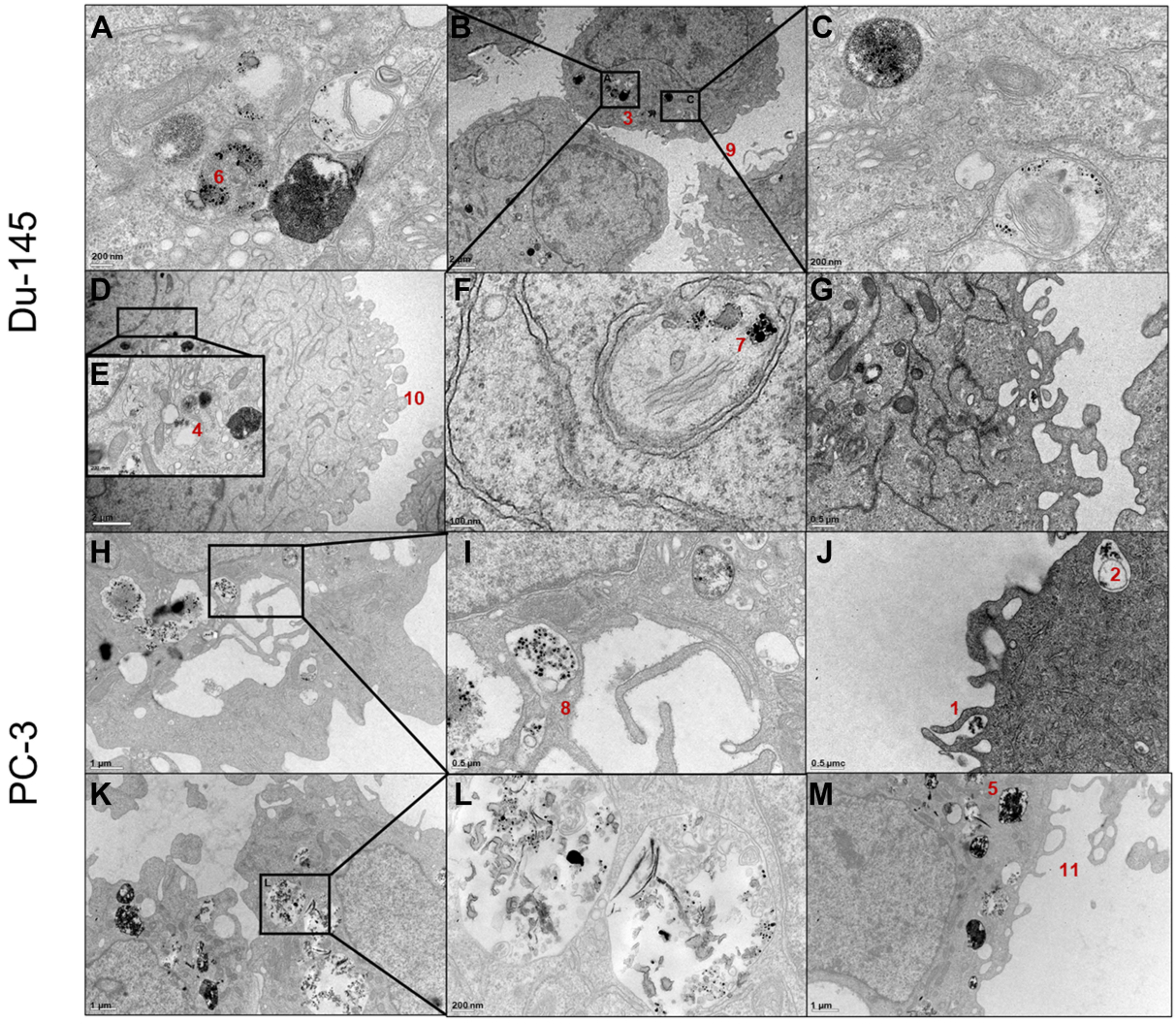

Figure 4 TEM images of Du-145 cells treated with IC_{25} of AgNPs (**A**–**C**) or G-AgNPs (**D**–**G**) and of PC-3 cells treated with IC_{25} of AgNPs (**H**–**J**) and G-AgNPs (**K**–**M**). From each sample, three pictures were taken with different ampliations. Thus, scale bars in B and D are 2μm, in H, K and M are 1μm, in G, I and J are 0.5 μm, in A, C, E and L are 200 nm and in F is 100 nm. 1 – Nanoparticles entering the cells through endocitosis; 2 – Nanoparticles trapped in lysosomes; 3 – Nanoparticles dispersed throughout the cytoplasm; 4 – Nanoparticles localized in the nucleus; 5 – Nanoparticles localized in the mitochondria; 6–8 – Nanoparticles maintain the monodispersed nature inside the cell; 9–11 – Membrane blebbing of the cells.

cytoplasm (Figure 4B-3), close to the nucleus (Figure 4E-4) and close to mitochondria (Figure 4M-5). It is important to observe that both nanoparticles remain monodispersed inside the cell, even if highly concentrated in the lysosomes (Figure 4A-6, F-7 and I-8). Additionally, in both cells, there is evidence of membrane blebbing, a known apoptotic feature (Figure 4B-9, D-10 and M-11).

AgNPs and G-AgNPs' Effect in Cellular Proliferation

To analyze the cellular proliferation after administration of the NPs, the BrdU assay was performed. In the Du-145 cell line, the IC_{25} and IC_{50} of AgNPs were able to inhibit the proliferation of the cells to 33.05% and 27.21%, respectively (Figure 5A and B). Regarding G-AgNPs, the IC_{25} and IC_{50} were able to inhibit proliferation of the cells to 27.21% and 14.12%, respectively (Figure 5A and B). In the PC-3 cell line, the IC_{25} and IC_{50} of AgNPs were able to inhibit the proliferation of the cells to 43.65% and 25.68%, respectively (Figure 5C and D). Regarding G-AgNPs, the IC_{25} and IC_{50} were able to inhibit proliferation of the cells to 34.84% and 19.21%, respectively (Figure 5C and D). Interestingly, for both IC_{25} and IC_{50}, G-AgNPs had a significantly higher power of cellular proliferation inhibition when compared to

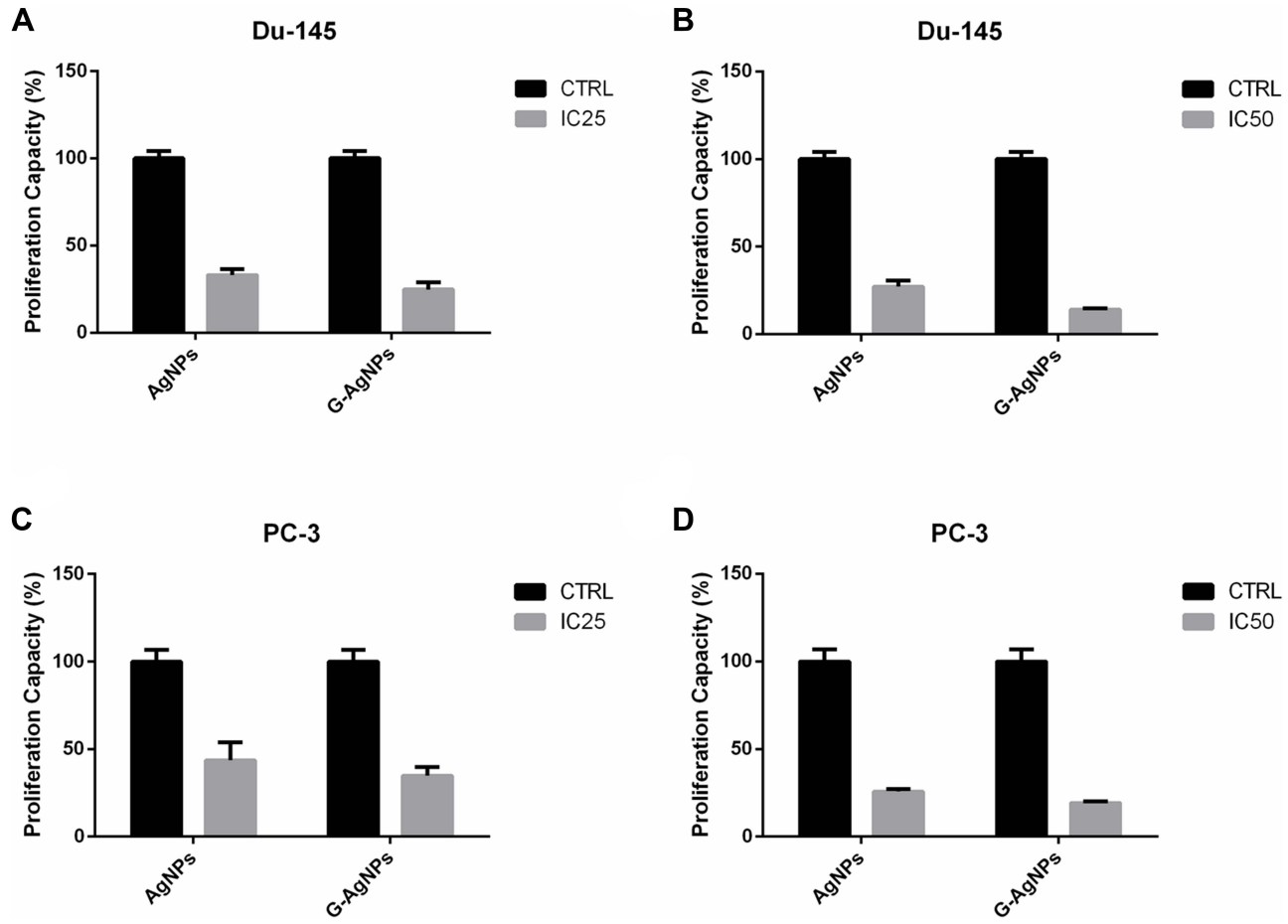

Figure 5 Evaluation of cell proliferation, by BrDu Assay, upon treatment with AgNPs and G-AgNPs in the Du-145 cell line using the determined IC_{25} (**A**) and the determined IC_{50} (**B**); and in the PC-3 cell line using the determined IC_{25} (**C**) and the determined IC_{50} (**D**). Results are expressed as percentage of control (untreated cells), as mean ± SEM.

AgNPs (24.85% vs 33.05%, p = 0.009 for IC_{25} and 14.12% vs 27.21%, p<0.001 in Du-145 cell line and 34.84% vs 43.65%, p=0.125 and 19.21% vs 25.68%, p<0.001 in PC-3 cell line).

AgNPs and G-AgNPs' Effect in Cell Cycle

To analyze possible cell cycle disruption following AgNPs or G-AgNPs administration, propidium iodide (PI) staining analysis by flow cytometry was used and further evaluation of the apoptosis status of the cells was performed (Figure 6).

In the Du-145 cell line, the IC_{25} of AgNPs and G-AgNPs increased the number of cells in the S phase (28.62% vs 18.94% and 24.93% vs 18.94%, respectively) and subsequently decreased the number of cells in G2/M (10.1% vs 14.61% and 9.27% vs 14.61%, respectively). Additionally, there was a significant increase in the number of cells in subG0 phase for both IC_{25} of AgNPs and G-AgNPs (4.23% vs 0.89% and 3.19% vs 0.89%). This effect was also observed for the IC_{50} of AgNPs and G-AgNPs, with more accentuated differences. There was an increase in the number of cells in the S phase (40.51% vs 18.94% and 32.02% vs 18.94%, respectively) and subsequent decrease the number of cells in G2/M phase (5.28% vs 14.61% and 6.21% vs 14.61%, respectively). The number of cells in subG0 phase for both AgNPs and in G-AgNPs was significantly higher (43.23% vs 0.89% and 53.09% vs 0.89%). Regarding the PC-3 cell lines, the same effect was observed: the IC_{25} of AgNPs and G-AgNPs increased the number of cells in the S phase (33.26% vs 12.65% and 38.21% vs 12.65%, respectively) and subsequently decreased the number of cells in G2/M (14.53% vs 26.53% and 11.08% vs 26.53%, respectively). This trend was also observed for the IC_{50} of AgNPs and G-AgNPs, with more accentuated differences. There was an increase in the number of cells in the S phase (42.06% vs

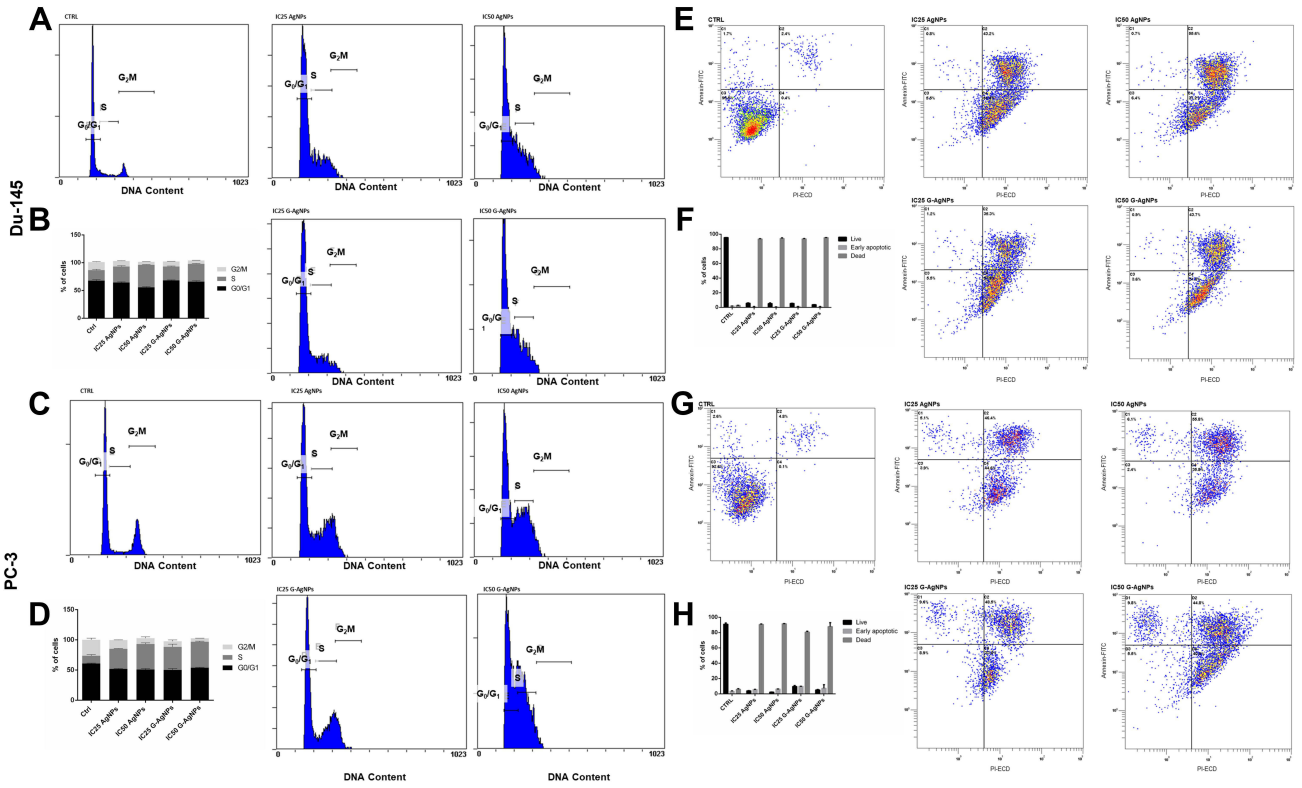

Figure 6 (**A**) Representative DNA histograms of cell cycle analysis assessed using a PI stain and flow cytometry of Du-145 cells treated with AgNPs and G-AgNPs in the determined IC_{25} and IC_{50}; (**B**) quantitative analysis of cell cycle disruptions of Du-145 cells treated with AgNPs and G-AgNPs in the determined IC_{25} and IC_{50}; (**C**) Representative DNA histograms of cell cycle analysis assessed using a PI stain and flow cytometry of PC-3 cells treated with AgNPs and G-AgNPs in the determined IC_{25} and IC_{50}; (**D**) Quantitative analysis of cell cycle disruptions of PC-3 cells treated with AgNPs and G-AgNPs in the determined IC_{25} and IC_{50}; (**E**) Representative flow cytometry images of apoptosis evaluation in Du-145 cells treated with AgNPs and G-AgNPs in the determined IC_{25} and IC_{50}; (**F**) Quantitative analysis of live, early apoptotic and dead cells of Du-145 cells treated with AgNPs and G-AgNPs in the determined IC_{25} and IC_{50}; (**G**) Representative flow cytometry images of apoptosis evaluation in PC-3 cells treated with AgNPs and G-AgNPs in the determined IC_{25} and IC_{50}; (**H**) Quantitative analysis of live, early apoptotic and dead cells of PC-3 cells treated with AgNPs and G-AgNPs in the determined IC_{25} and IC_{50}. Data are expressed as mean ± SEM.

10.30% and 42.89% vs 10.30%, respectively) and subsequently decrease in the number of cells in G2/M phase (9.17% vs 22.39% and 5.78% vs 22.39%, respectively). Furthermore, when the apoptotic state of the cells was assessed one can see that most cells marked positive for Annexin and PI confirming their apoptotic state after administration of both AgNPs and G-AgNPs.

AgNPs and G-AgNPs' Increase Cells' ROS Production

To analyze ability of the NPs to induce reactive oxygen species (ROS) production by cells, the DCFH2-DA assay was performed. In the Du-145 cell line, the IC_{25} and IC_{50} of AgNPs were able to induce about 2.1- and 2.8-fold increase in the cell mean fluorescence compared to control, respectively (Figure 7A and B). Regarding G-AgNPs, they have a similar effect when compared to AgNPs, with a fold increase in the cell mean fluorescence related to control of about 2.0 and 2.7, for the IC_{25} and the IC_{50}, respectively (Figure 7C and D). In the PC-3 cell line, the IC_{25} and IC_{50} of AgNPs were able to increase the cell mean fluorescence to 2.2- and 2.8-fold increase compared to control cells, respectively (Figure 7E and F). Regarding G-AgNPs, the IC_{25} have a similar effect of AgNPs IC_{25} (2.2-fold increase) and the IC_{50} were able to increase the cell mean fluorescence of 2.3-fold increase when compared to control (Figure 7G and H).

AgNPs and G-AgNPs' Effect in Mitochondria Depolarization

To analyze the mitochondria membrane damage after administration of the NPs, the TMRE assay was performed. Since this dye is positively charged, it accumulates in the negatively charged mitochondria. When mitochondria is depolarized, its membrane potential decreases and it does not incorporate the dye (Figure 8C and F). In the Du-145 cell line, the IC_{25} and

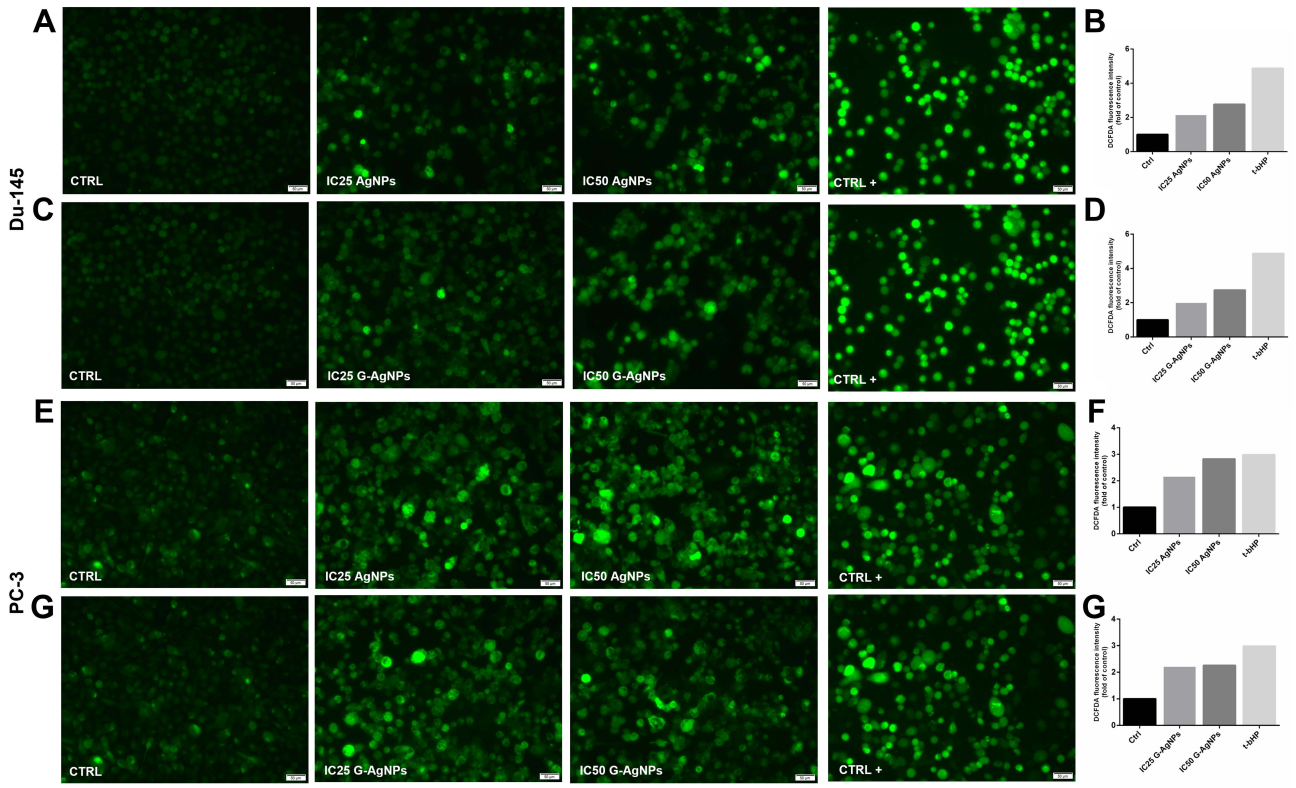

Figure 7 Evaluation of ROS production, by DCFH2-DA Assay, in the Du-145 cell line upon treatment with the determined IC_{25} and IC_{50} AgNPs (**A** and **B**) and upon treatment with the determined IC_{25} and IC_{50} G-AgNPs (**C** and **D**); and in the PC-3 cell line upon treatment with the determined IC_{25} and IC_{50} AgNPs (**E** and **F**) and upon treatment with the determined IC_{25} and IC_{50} G-AgNPs (**G** and **H**). (**A, C, E** and **G**) Representative images (10×) of DCFH2-DA labeled mitochondria (Photographs taken using an Olympus IX51 microscope). (**B, D, F** and **H**) Graphical representation of the DCFH2-DA fluorescence signal intensity in the different tested conditions. T-bhp is used as positive control. Results are expressed as percentage of control (untreated cells), as mean ± SEM.

IC_{50} of AgNPs were able to depolarize the cells' mitochondria to 32.74% and 10.36%, respectively (Figure 8A and B). Regarding G-AgNPs, the IC_{25} and the IC_{50} were able to depolarize the cells' mitochondria to 30.13% and 6.96%, respectively (Figure 8A and B). In the PC-3 cell line, the IC_{25} and IC_{50} of AgNPs were able to depolarize the cells' mitochondria to 49.54% and 49.39%, respectively (Figure 8D and E). Regarding G-AgNPs, the IC_{25} and IC_{50} were able to depolarize the mitochondria of the cells to 47.45% and 38.13, respectively (Figure 8D and E). Interestingly, for IC_{50}, after G-AgNPs administration, there were significantly less cells with polarized mitochondria than after AgNPs administration in the PC-3 cell line (38.13% vs 49.39%, $p = 0.012$).

Discussion

The poor prognosis, short overall survival, and the low quality of life of CRPC patients added to the limited therapeutic options available are major concerns in PCa management and make the development of new therapeutic strategies imperative.[6] The mechanism behind the acquisition of resistance to hormone therapy in patients that progress to CRPC is complex and not completely understood, but the importance of glucose metabolism deregulation has already been shown, and can be used as an advantage for the development of new therapeutic approaches.[16] In the last years, the development of metallic nanoparticles has raised increased interest in the scientific community and AgNPs, specifically, have already shown cytotoxic potential in different tumor models.[25,36–38] The increased glucose consumption in more advanced forms of PCa can be an opportunity to design AgNPs that specifically target cancer cells, through a glucose functionalization.

In the present study, AgNPs were successfully synthesized and further functionalized with glucosamine, showing physical and chemical characteristics that optimize their uptake by cancer cells and, consequently, their cytotoxic capacity. The small size, spherical shape and monodisperse nature of these NPs promotes their internalization and intracellular bioavailability. In fact, spherical NPs have been shown to have a higher internalization than asymmetrically

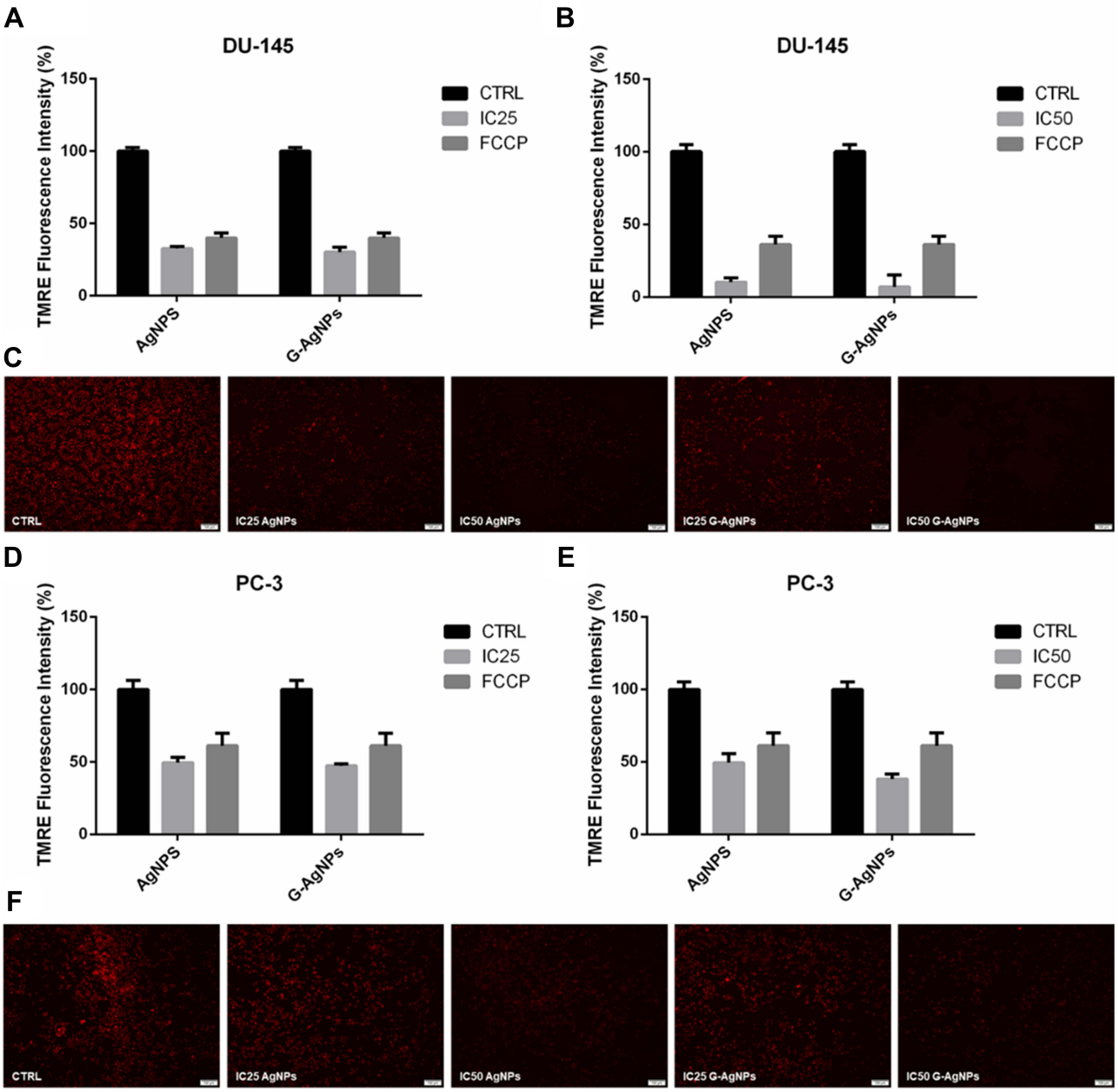

Figure 8 Evaluation of mitochondria membrane depolarization, by TMRE Assay, upon treatment with AgNPs and G-AgNPs in the Du-145 cell line (**C**) using the determined IC_{25} (**A**) and the determined IC_{50} (**B**); and in the PC-3 cell line (**F**) using the determined IC_{25} (**D**) and the determined IC_{50} (**E**). Representative images (10×) of TMRE labeled mitochondria (Photographs taken using an Olympus IX51 microscope). Results are expressed as percentage of control (untreated cells), as mean ± SEM.

shaped ones, and smaller-sized AgNPs have shown a higher uptake and cytotoxicity because of their increased surface area and particle number for the same mass/volume dose.[39] Additionally, the demonstrated stability of these NPs in cell culture medium is of great advantage because, contrary to small-molecule drugs, nanoscale drugs slowly leak from blood vessels after intravenous induction, thus their accumulation into the tumor would not be efficient if they were unstable in serum.[40]

Both AgNPs and G-AgNPs had cytotoxic effects only on the hormone-resistant cells Du-145 and PC-3 and not to the hormone-sensitive cell line LNCaP, even when high concentrations of the NPs were administered. The different molecular profile of these cell lines apart from the absence of AR signal in both Du-145 and PC-3 can be the explanation behind this selective effect. Interestingly, Alvin Y. Liu has shown that the LNCaP cell line displays a very different cell

surface molecule profile from Du-145 and PC-3 cells (which are much more similar between them), which may lead to different internalization of the AgNPs.[41] In fact, LNCaP cells do not express both caveolin-1 and caveolin-2, contrarily to Du-145 and PC-3.[42] These molecules mediate the independent-clathrin pathway of endocytosis via caveolae, a ligand-triggered mechanism that leads to a more selective uptake and that may be behind the uptake of the synthesized nanoparticles and the absence of effect in the LNCaP cell line.[43]

We also reported a higher cytotoxic effect and proliferation blockage of G-AgNPs in both PC-3 and Du-145, which show a lower IC_{25} and IC_{50} when compared with AgNPs. This higher effect can be explained by the different metabolic nature of hormone-resistant cells (Du-145 and PC-3). Previous studies have shown that these two cell lines show a metabolic shift towards the Warburg Effect, displaying lower consumption of O_2, higher rates of lactate production and higher glucose consumption rates which may favor the uptake of the NPs.[44,45] In fact, Effert et al have already shown that GLUT-1′s mRNA expression is higher in Du-145 and PC3, when compared with LNCaP cell line.[46] Interestingly, calveolin-1 has been shown to be involved in glucose metabolism, namely in the Warburg Effect and to enhance glucose uptake in prostate cancer cells.[47] This can explain the higher effect of G-AgNPs and may suggest that they are preferably uptaked by cells with high glucose consumption and calveolin expression. This would be an advantage in a systemic administration of the nanoparticles such as the CRPC context, since they would be preferably uptaked by these cells, which can allow a more directed effect.

To date, there are several studies reporting the effect of AgNPs synthesized by different methods and with a variety of cappings and their cytotoxic effect in PCa cell lines.[48–63] Among these studies, the mechanism of action is, most of the times, common to the one we found in the present study, with an increase in ROS production, mitochondrial damage, nuclear fragmentation and cell apoptosis.[50,52,60,62,63] However, most of them do not compare AgNPs' effect in hormone-sensitive and hormone-resistant cell lines and, to the best of our knowledge, the present study is the first one reporting the effect of AgNPs with a glucose functionalization in PCa and with a selective effect towards hormone resistance in this tumor model.

To better understand the observed cytotoxic effect, we performed a TEM analysis of the NPs location in the cells and several phenotypic assays. Firstly, we confirmed that the NPs enter the cells through endocytosis and targeted to lysosomes. In fact, lysosomes have in their composition a variety of hydrolytic enzymes and an acidic environment which will degrade AgNPs capping and release Ag^+, a mechanism called "lysosome-enhanced Trojan horse effect".[64] Moreover, it was already reported that AgNPs, when interacting with the acidic lysosomal compartment, induce the production of several ROS (superoxide anions (O_2^-), hydroxyl radicals ($^{\bullet}OH$), and hydrogen peroxide (H_2O_2), which explains the increase in ROS production observed after treatment with NPs.[39] The diffusion of these ROS into cytoplasm leads to oxidative damage in different organelles such as mitochondria. In the present study, a depolarization of the mitochondrial membrane of Du-145 and PC-3 was observed when treated with both NPs. We have also observed a S-Phase cell cycle arrest after treatment with AgNPs and G-AgNPs. The successful progression through cell cycle is mediated by different proteins, cyclins, cyclin-dependent kinases and their inhibitors, being this strict regulation responsible for guaranteeing the safe progression through DNA replication and division.[65] The S-phase checkpoint checks the fidelity of DNA replication confirming there are no areas of unrepaired DNA damage from earlier cell cycle points.[66] Thus, the S-phase arrest shown in our study can be indicative of DNA damage and, along with the increased ROS production and mitochondrial damage can support the blockage of cellular proliferation observed and lead to the apoptotic state of the cells which we observed through FITC annexin V and PI staining.

Conclusions

In this study, we successfully designed AgNPs with a glucose functionalization that selectively induce damage in CRPC cells (as opposed to hormone-sensitive ones). The effect of the NPs was higher after functionalization, showing the potential of glucose to favor the uptake of the AgNPs by cancer cells. To the best of our knowledge, this was the first study reporting a selective effect of AgNPs directed to CRPC and the effect of glucose functionalization of AgNPs in PCa. This study shows the potential of these AgNPs as a new therapeutic approach to castration-resistant prostate cancer that needs to be validated in 3D cell cultures to understand the penetration ability of the NPs and in vivo to confirm the results and study the delivery and excretion pathways' safety. Additionally, exploring the molecular profile, including the

expression of calveolins, of the three cell lines could be of use to explain the differences of AgNP's effect. Nevertheless, the present results are very promising and these NPs could be a potential therapeutic strategy and improve the management of patients with PCa resistant to hormone therapy or with the presence of metastasis.

Abbreviations

ADT, androgen deprivation therapy; AgNPs, silver nanoparticles; AR, androgen receptor; BrdU, bromodeoxyuridine; CRPC, castration-resistant prostate cancer; DLS, dynamic light scattering; EMA, European Medicines Agency; FTIR, Fourier transform infrared spectroscopy; G-AgNPs, AgNPs functionalized with glucose; H_2DCFDA, 2',7'-dichlorodihydrofluorescein diacetate; IC, inhibitory concentration; MQ, MilliQ; NPs, nanoparticles; OS, overall survival; PCa, prostate cancer; PI, propidium iodide; ROS, reactive oxygen species; SEM, standard error of mean; TEM, transmission electron microscopy; TMRE, tetramethylrhodamine, ethyl ester.

Funding

This research was funded by the National Funds (FCT, Fundação para a Ciência e a Tecnologia) through project PTDC/MED-QUI/29800/2017 and in part by Program a Operacional Regional do Norte and co-funded by European Regional Development Fund under the project "The Porto Comprehensive Cancer Center" with the reference NORTE-01-0145-FEDER-072678- Consórcio PORTO.CCC – Porto. Comprehensive Cancer Center. MM is funded by FCT through the grant 2020.08193.BD, VM is funded by RNCCC/P.CCC/CI-IPOP/Lab2/InvJun under the project NORTE-01-0145-FEDER-072678 and FD is funded by UIDP/00776/2020-4B.

Disclosure

The authors report no conflicts of interest in this work.

References

1. Rawla P. Epidemiology of prostate cancer. *World J Oncol*. 2019;10(2):63–89. doi:10.14740/wjon1191
2. Sung H, Ferlay J, Siegel RL, et al. Global cancer statistics 2020: GLOBOCAN estimates of incidence and mortality worldwide for 36 cancers in 185 countries. *CA Cancer J Clin*. 2021;71:209–249. doi:10.3322/caac.21660
3. Lim MCJ, Baird A-M, Greene J, et al. hsa_circ_0001275 is one of a number of circRNAs dysregulated in enzalutamide resistant prostate cancer and confers enzalutamide resistance in vitro. *Cancers*. 2021;13(24):6383. doi:10.3390/cancers13246383
4. Mottet N, Bellmunt J, Bolla M, et al. EAU-ESTRO-SIOG guidelines on prostate cancer. part 1: screening, diagnosis, and local treatment with curative intent. *Eur Urol*. 2017;71(4):618–629. doi:10.1016/j.eururo.2016.08.003
5. Gandhi J, Afridi A, Vatsia S, et al. The molecular biology of prostate cancer: current understanding and clinical implications. *Prostate Cancer Prostatic Dis*. 2018;21(1):22–36. doi:10.1038/s41391-017-0023-8
6. Crowley F, Sterpi M, Buckley C, Margetich L, Handa S, Dovey Z. A review of the pathophysiological mechanisms underlying castration-resistant prostate cancer. *Res Rep Urol*. 2021;13:457–472. doi:10.2147/RRU.S264722
7. Dong L, Zieren RC, Xue W, de Reijke TM, Pienta KJ. Metastatic prostate cancer remains incurable, why? *Asian J Urol*. 2019;6(1):26–41. doi:10.1016/j.ajur.2018.11.005
8. Naseer F, Ahmad T, Kousar K, Anjum S. Advanced therapeutic options for treatment of metastatic castration resistant prostatic adenocarcinoma. *Front Pharmacol*. 2021;12. doi:10.3389/fphar.2021.728054
9. McNevin CS, Baird AM, McDermott R, Finn SP. Diagnostic strategies for treatment selection in advanced prostate cancer. *Diagnostics*. 2021;11(2):345. doi:10.3390/diagnostics11020345
10. Powers E, Karachaliou GS, Kao C, et al. Novel therapies are changing treatment paradigms in metastatic prostate cancer. *J Hematol Oncol*. 2020;13(1):144. doi:10.1186/s13045-020-00978-z
11. Hu C-Y, Wu K-Y, Lin T-Y, Chen -C-C. The crosstalk of long non-coding RNA and microRNA in castration-resistant and neuroendocrine prostate cancer: their interaction and clinical importance. *Int J Mol Sci*. 2022;23(1):392. doi:10.3390/ijms23010392
12. Wang J, Xu W, Wang B, et al. GLUT1 is an AR target contributing to tumor growth and glycolysis in castration-resistant and enzalutamide-resistant prostate cancers. *Cancer Lett*. 2020;485:45–55. doi:10.1016/j.canlet.2020.05.007
13. Cui Y, Nadiminty N, Liu C, Lou W, Schwartz CT, Gao AC. Upregulation of glucose metabolism by NF-κB2/p52 mediates enzalutamide resistance in castration-resistant prostate cancer cells. *Endocr Relat Cancer*. 2014;21(3):435–442. doi:10.1530/ERC-14-0107
14. Verma S, Shankar E, Chan ER, Gupta S. Metabolic reprogramming and predominance of solute carrier genes during acquired enzalutamide resistance in prostate cancer. *Cells*. 2020;9(12):2535. doi:10.3390/cells9122535
15. Tsouko E, Khan AS, White MA, et al. Regulation of the pentose phosphate pathway by an androgen receptor–mTOR-mediated mechanism and its role in prostate cancer cell growth. *Oncogenesis*. 2014;3(5):e103–e103. doi:10.1038/oncsis.2014.18
16. Morais MDF, Prior J, Teixeira AL, Medeiros R. *The Impact of Oxidoreductases-Related MicroRNAs in Glucose Metabolism of Renal Cell Carcinoma and Prostate Cancer*. IntechOpen; 2021.

17. Cardoso HJ, Carvalho TMA, Fonseca LRS, Figueira MI, Vaz CV, Socorro S. Revisiting prostate cancer metabolism: from metabolites to disease and therapy. *Med Res Rev*. 2021;41(3):1499–1538. doi:10.1002/med.21766
18. Cutruzzolà F, Giardina G, Marani M, et al. Glucose metabolism in the progression of prostate cancer. *Front Physiol*. 2017;8:97. doi:10.3389/fphys.2017.00097
19. Pereira-Nunes A, Simões-Sousa S, Pinheiro C, Miranda-Gonçalves V, Granja S, Baltazar F. Targeting lactate production and efflux in prostate cancer. *Biochimica et Biophysica Acta*. 2020;1866:165894. doi:10.1016/j.bbadis.2020.165894
20. Liberti MV, Locasale JW. The Warburg Effect: how does it benefit cancer cells? *Trends Biochem Sci*. 2016;41(3):211–218. doi:10.1016/j.tibs.2015.12.001
21. Gherasim O, Puiu RA, Bîrcă AC, Burduşel AC, Grumezescu AM. An updated review on silver nanoparticles in biomedicine. *Nanomaterials*. 2020;10(11):2318. doi:10.3390/nano10112318
22. Figueiredo P, Bauleth-Ramos T, Hirvonen J, Sarmento B, Santos HA. Chapter 1 - the emerging role of multifunctional theranostic materials in cancer nanomedicine. In: Conde J, editor. *Handbook of Nanomaterials for Cancer Theranostics*. Elsevier; 2018:1–31.
23. Chiang C-L, Cheng M-H, Lin C-H. From nanoparticles to cancer nanomedicine: old problems with new solutions. *Nanomaterials*. 2021;11(7):1727. doi:10.3390/nano11071727
24. Kowalczyk P, Szymczak M, Maciejewska M, et al. All that glitters is not silver—a new look at microbiological and medical applications of silver nanoparticles. *Int J Mol Sci*. 2021;22(2):854. doi:10.3390/ijms22020854
25. Morais M, Teixeira AL, Dias F, Machado V, Medeiros R, Prior JAV. Cytotoxic effect of silver nanoparticles synthesized by green methods in cancer. *J Med Chem*. 2020;63(23):14308–14335. doi:10.1021/acs.jmedchem.0c01055
26. Andleeb A, Andleeb A, Asghar S, et al. A systematic review of biosynthesized metallic nanoparticles as a promising anti-cancer-strategy. *Cancers*. 2021;13(11):2818. doi:10.3390/cancers13112818
27. Ivlieva A, Petritskaya E, Rogatkin D, et al. Does nanosilver have a pronounced toxic effect on humans? *Appl Sci*. 2022;12(7):3476. doi:10.3390/app12073476
28. Maziero JS, Thipe VC, Rogero SO, et al. Species-specific in vitro and in vivo evaluation of toxicity of silver nanoparticles stabilized with gum Arabic protein. *Int J Nanomedicine*. 2020;15:7359–7376. doi:10.2147/IJN.S250467
29. Bastús NG, Merkoçi F, Piella J, Puntes V. Synthesis of highly monodisperse citrate-stabilized silver nanoparticles of up to 200 nm: kinetic control and catalytic properties. *Chem Mater*. 2014;26(9):2836–2846. doi:10.1021/cm500316k
30. Ashraf JM, Ansari MA, Khan HM, Alzohairy MA, Choi I. Green synthesis of silver nanoparticles and characterization of their inhibitory effects on AGEs formation using biophysical techniques. *Sci Rep*. 2016;6(1):20414. doi:10.1038/srep20414
31. Uznanski P, Zakrzewska J, Favier F, Kazmierski S, Bryszewska E. Synthesis and characterization of silver nanoparticles from (bis)alkylamine silver carboxylate precursors. *J Nanoparticle Res*. 2017;19(3):121. doi:10.1007/s11051-017-3827-5
32. Ayodhya D, Veerabhadram G. One-pot, aqueous synthesis of multifunctional biogenic Ag NPs for efficient 4-NP reduction, Hg2+ detection, bactericidal, and antioxidant activities. *Inorganic Nano Metal Chem*. 2021;51(12):1831–1841.
33. Aggarwal P, Hall JB, McLeland CB, Dobrovolskaia MA, McNeil SE. Nanoparticle interaction with plasma proteins as it relates to particle biodistribution, biocompatibility and therapeutic efficacy. *Adv Drug Deliv Rev*. 2009;61(6):428–437. doi:10.1016/j.addr.2009.03.009
34. Rampado R, Crotti S, Caliceti P, Pucciarelli S, Agostini M. Recent advances in understanding the protein corona of nanoparticles and in the formulation of "stealthy" nanomaterials. *Front Bioengine Biotechnol*. 2020;8. doi:10.3389/fbioe.2020.00166
35. Moore TL, Rodriguez-Lorenzo L, Hirsch V, et al. Nanoparticle colloidal stability in cell culture media and impact on cellular interactions. *Chem Soc Rev*. 2015;44(17):6287–6305. doi:10.1039/C4CS00487F
36. Rank Miranda R, Pereira da Fonseca M, Korzeniowska B, Skytte L, Lund Rasmussen K, Kjeldsen F. Elucidating the cellular response of silver nanoparticles as a potential combinatorial agent for cisplatin chemotherapy. *J Nanobiotechnology*. 2020;18(1):164. doi:10.1186/s12951-020-00719-x
37. Muhammad N, Zhao H, Song W, et al. Silver nanoparticles functionalized Paclitaxel nanocrystals enhance overall anti-cancer effect on human cancer cells. *Nanotechnology*. 2021;32(8):085105. doi:10.1088/1361-6528/abcacb
38. Zhao Q, Sun XY, Wu B, et al. Construction of biomimetic silver nanoparticles in the treatment of lymphoma. *Mater Sci Engine C*. 2021;119:111648. doi:10.1016/j.msec.2020.111648
39. Panzarini E, Mariano S, Carata E, Mura F, Rossi M, Dini L. Intracellular transport of silver and gold nanoparticles and biological responses: an update. *Int J Mol Sci*. 2018;19(5):1305. doi:10.3390/ijms19051305
40. Kobayashi H, Watanabe R, Choyke PL. Improving conventional enhanced permeability and retention (EPR) effects; what is the appropriate target? *Theranostics*. 2013;4(1):81–89. doi:10.7150/thno.7193
41. Liu AY. Differential expression of cell surface molecules in prostate cancer cells. *Cancer Res*. 2000;60(13):3429–3434.
42. Kamibeppu T, Yamasaki K, Nakahara K, et al. Caveolin-1 and −2 regulate cell motility in castration-resistant prostate cancer. *Res Rep Urol*. 2018;10:135–144. doi:10.2147/RRU.S173377
43. Kiss AL, Botos E. Endocytosis via caveolae: alternative pathway with distinct cellular compartments to avoid lysosomal degradation? *J Cell Mol Med*. 2009;13(7):1228–1237. doi:10.1111/j.1582-4934.2009.00754.x
44. Higgins LH, Withers HG, Garbens A, et al. Hypoxia and the metabolic phenotype of prostate cancer cells. *Biochimica et Biophysica Acta*. 2009;1787(12):1433–1443. doi:10.1016/j.bbabio.2009.06.003
45. Pertega-Gomes N, Felisbino S, Massie CE, et al. A glycolytic phenotype is associated with prostate cancer progression and aggressiveness: a role for monocarboxylate transporters as metabolic targets for therapy. *J Pathol*. 2015;236(4):517–530. doi:10.1002/path.4547
46. Effert P, Beniers AJ, Tamimi Y, Handt S, Jakse G. Expression of glucose transporter 1 (Glut-1) in cell lines and clinical specimens from human prostate adenocarcinoma. *Anticancer Res*. 2004;24(5a):3057–3063.
47. Nwosu ZC, Ebert MP, Dooley S, Meyer C. Caveolin-1 in the regulation of cell metabolism: a cancer perspective. *Mol Cancer*. 2016;15(1):71. doi:10.1186/s12943-016-0558-7
48. He Y, Du Z, Ma S, et al. Biosynthesis, antibacterial activity and anticancer effects against prostate cancer (PC-3) cells of silver nanoparticles using dimocarpus longan lour. peel extract. *Nanoscale Res Lett*. 2016;11(1):300. doi:10.1186/s11671-016-1511-9
49. Firdhouse MJ, Lalitha P. Biosynthesis of silver nanoparticles using the extract of Alternanthera sessilis—antiproliferative effect against prostate cancer cells. *Cancer Nanotechnol*. 2013;4(6):137–143. doi:10.1007/s12645-013-0045-4

50. Bethu MS, Netala VR, Domdi L, Tartte V, Janapala VR. Potential anticancer activity of biogenic silver nanoparticles using leaf extract of Rhynchosia suaveolens: an insight into the mechanism. *Artif Cells, Nanomed Biotechnol*. 2018;46(sup1):104–114. doi:10.1080/21691401.2017.1414824
51. Netala VR, Bukke S, Domdi L, et al. Biogenesis of silver nanoparticles using leaf extract of Indigofera hirsuta L. and their potential biomedical applications (3-in-1 system). *Artif Cells, Nanomed Biotechnol*. 2018;46(sup1):1138–1148. doi:10.1080/21691401.2018.1446967
52. Zhang K, Liu X, Samuel Ravi SOA, et al. Synthesis of silver nanoparticles (AgNPs) from leaf extract of Salvia miltiorrhiza and its anticancer potential in human prostate cancer LNCaP cell lines. *Artif Cells, Nanomed Biotechnol*. 2019;47(1):2846–2854. doi:10.1080/21691401.2019.1638792
53. Jadhav K, Deore S, Dhamecha D, et al. Phytosynthesis of silver nanoparticles: characterization, biocompatibility studies, and anticancer activity. *ACS Biomater Sci Engine*. 2018;4(3):892–899. doi:10.1021/acsbiomaterials.7b00707
54. El-Sheikh SMA, Edrees N, El-Sayed H, et al. Could cisplatin loading on biosynthesized silver nanoparticles improve its therapeutic efficacy on human prostate cancer cell line and reduce its in vivo nephrotoxic effects? *Biol Trace Elem Res*. 2021;200:582–590. doi:10.1007/s12011-021-02677-3
55. Gavamukulya Y, Maina EN, El-Shemy HA, et al. Annona muricata silver nanoparticles exhibit strong anticancer activities against cervical and prostate adenocarcinomas through regulation of CASP9 and the CXCL1/CXCR2 genes axis. *Tumour Biol*. 2021;43(1):37–55. doi:10.3233/TUB-200058
56. Bello BA, Khan SA, Khan JA, Syed FQ, Anwar Y, Khan SB. Antiproliferation and antibacterial effect of biosynthesized AgNps from leaves extract of Guiera senegalensis and its catalytic reduction on some persistent organic pollutants. *J Photochem Photobiol B*. 2017;175:99–108. doi:10.1016/j.jphotobiol.2017.07.031
57. He Y, Li X, Wang J, et al. Synthesis, characterization and evaluation cytotoxic activity of silver nanoparticles synthesized by Chinese herbal Cornus officinalis via environment friendly approach. *Environ Toxicol Pharmacol*. 2017;56:56–60. doi:10.1016/j.etap.2017.08.035
58. Kang JS, Park JW. Insight on cytotoxic effects of silver nanoparticles: alternative androgenic transactivation by adsorption with DHT. *Sci Total Environ*. 2018;618:712–717. doi:10.1016/j.scitotenv.2017.08.059
59. Chen Y, Yang T, Chen S, Qi S, Zhang Z, Xu Y. Silver nanoparticles regulate autophagy through lysosome injury and cell hypoxia in prostate cancer cells. *J Biochem Mol Toxicol*. 2020;34(5):e22474. doi:10.1002/jbt.22474
60. Prasannaraj G, Sahi SV, Ravikumar S, Venkatachalam P. Enhanced cytotoxicity of biomolecules loaded metallic silver nanoparticles against human liver (HepG2) and prostate (PC3) cancer cell lines. *J Nanosci Nanotechnol*. 2016;16(5):4948–4959. doi:10.1166/jnn.2016.12336
61. Gavamukulya Y, Maina EN, Meroka AM, El-Shemy HA, Magoma G, Wamunyokoli F. In search of new anticancer drugs: data for cytotoxic activities of green synthesized silver nanoparticles from ethanolic extracts of fruits and leaves of Annona muricata and 5-fluorouracil against HeLa, PC3 and PNT1A cell lines. *Data Brief*. 2019;26:104442. doi:10.1016/j.dib.2019.104442
62. Kumari R, Saini AK, Kumar A, Saini RV. Apoptosis induction in lung and prostate cancer cells through silver nanoparticles synthesized from Pinus roxburghii bioactive fraction. *J Biol Inorganic Chem*. 2020;25(1):23–37. doi:10.1007/s00775-019-01729-3
63. Singh SP, Mishra A, Shyanti RK, Singh RP, Acharya A. Silver nanoparticles synthesized using carica papaya leaf extract (AgNPs-PLE) causes cell cycle arrest and apoptosis in human prostate (DU145) cancer cells. *Biol Trace Elem Res*. 2021;199(4):1316–1331. doi:10.1007/s12011-020-02255-z
64. Hsiao IL, Hsieh YK, Wang CF, Chen IC, Huang YJ. Trojan-horse mechanism in the cellular uptake of silver nanoparticles verified by direct intra- and extracellular silver speciation analysis. *Environ Sci Technol*. 2015;49(6):3813–3821. doi:10.1021/es504705p
65. Ferenbach DA, Bonventre JV. Chapter 27 - the molecular response to renal injury: how does chronic renal damage suppress normal repair processes? In: Little MH, editor. *Kidney Development, Disease, Repair and Regeneration*. San Diego: Academic Press; 2016:367–379.
66. Johnson DG, Walker CL. Cyclins and cell cycle checkpoints. *Annu Rev Pharmacol Toxicol*. 1999;39:295–312. doi:10.1146/annurev.pharmtox.39.1.295